ACS APPLIED MATERIALS & INTERFACES

Research Article

www.acsami.org

Superstrate $CuInS_2$ Photovoltaics with Enhanced Performance Using a CdS/ZnO Nanorod Array

Dongwook Lee and Kijung Yong*

Surface Chemistry Laboratory of Electronic Materials (SCHEMA), Department of Chemical Engineering, POSTECH, Pohang 790-784, Korea

ABSTRACT: An air-stable, low-temperature, solution-based process for preparing $CuInS_2$ (CIS) superstrate solar cells using CdS-decorated ZnO nanorod (NR) arrays is reported. Efficient light harvesting and photoexcited charge transport were achieved by fabricating a ZnO NR window layer with a large p-n junction area via a hydrothermal reaction. A CdS buffer layer was deposited on a transparent ZnO NR substrate at room temperature via successive ion layer adsorption and reaction (SILAR) or nanocrystal layer deposition (NCLD). The prepared CdS/ZnO NR assembly was coated with a CIS absorber layer without the need for surface passivation organics or dispersion reagents. The CIS precursor solution, prepared using a metal salt, thiourea, and an amine solvent, yielded CIS nanocrystals (NCs) at temperatures up to 250 °C. The CIS/CdS/ZnO NR heterojunction structure exhibited an excellent photovoltaic performance compared to a planar ZnO film device due to enhanced light transmittance toward the absorber and a high charge collection efficiency. These results suggest that a superstrate CIS/CdS/ZnO NRs photovoltaic cell fabricated via the low-cost route described here has great potential as a next-generation solar cell device.

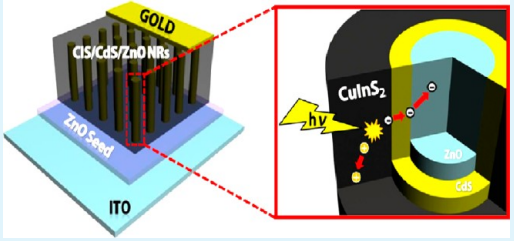

KEYWORDS: *ZnO, nanorod arrays, precursor solution, nanocrystal, thin film solar cell, superstrate*

1. INTRODUCTION

Solar energy provides a promising clean energy source as an alternative to hydrocarbon-based fossil fuel combustion, which produces serious detrimental effects, including global warming and air pollution. Recently, $Cu(InGa)(SeS)_2$ (CIGS) thin film solar cells were developed as a substitute for Si-based solar cells. CIGS solar cells displayed a high optical absorption coefficient, tunable band gap energy, long-term chemical stability, and a high efficiency.[1] Over the past few years, various approaches have been explored for achieving high-quality CIGS absorber thin films. The best such cell, prepared using vacuum-based deposition processes, has yielded a 20% power conversion efficiency.[2−5] Vacuum deposition methods have only limited applicability to the large-scale commercial production of thin film solar cells because vacuum equipment is expensive and the material use in such systems is inefficient. To overcome these obstacles to commercialization, several solution-based, low-temperature deposition methods have been investigated, including precursor solution growth and nanoparticle (NP) ink deposition.[6−8]

Molecular precursor solution methods rely on the direct coating of a solution containing metal (Cu, In, Ga) and chalcogen (Se, S) precursors in an amine or alcohol solvent and the subsequent heat treatment facilitates crystallization.[9−12] In some cases, a polymeric binder is added to achieve a desired rheology.[9,13] Recently, Liu et al. used a hydrazine-based precursor solution to obtain a remarkably high cell efficiency of 12%.[14] The use of hydrazine, a toxic flammable solution, and the need for numerous coating cycles limits the applicability of this approach. In the case of ink deposition techniques, hot-injection or solvothermal approaches using organic surfactants have been preferentially used for NP synthesis, permitting control over the NP size and composition.[15−18] Ink deposition is compatible with continuous printing processes because of its low deposition temperature; however, this approach generally requires complicated synthetic steps and inert atmospheric conditions, and it suffers from low yields and poor crystal quality. Additionally, the organic surfactant can deteriorate the transfer of photogenerated charge carriers among individual NPs.[19,20]

Recently, metal oxide nanostructures (e.g., ZnO, TiO_2, ITO) have been considered as promising constituent materials in various solar cells. Those 1D metal oxide nanostructures can be fabricated by economic solution-based process. Those ordered nanostructures increase light capture via diffused reflections between nanostructure arrays, and they enhance charge separation and transport via their unique inherent morphological, electrical, and optoelectronic properties (e.g., their high surface-to-volume ratio and high electron mobility).[21−23] However, to apply these advantages of 1D metal oxide nanostructures in CIGS thin film solar cells, superstrate cell structures are required, which are generally fabricated through a process that is the reverse of the process used to prepare conventional substrate cell structures. From a practical perspective, it is very difficult to penetrate the nanostructured buffer and window layers into densely crystallized solid phase of

Received: September 12, 2012
Accepted: November 19, 2012
Published: November 19, 2012

CIGS absorber film to form heterojunctions with large interfacial areas. For this reason, liquid phase precursor methods can be used to fill CIS between nanostructures. However, recently, the development of CIGS superstrate thin film solar cells with ordered nonabsorber nanostructures has not been extensively studied. A bulk heterojunction-type solar cell using sputter-grown indium tin oxide (ITO) NRs and drop-casted CIS NPs, reported by Cho et al., showed an increase in the photogenerated current relative to a film-type ITO.[23] Their device fabrication process includes several vacuum-based techniques such as atomic layer deposition (ALD) process and sputtering process at high temperature to grow TiO_2 layer and ITO nanorods. Recently, Zhang et al. described a CIS superstrate cell prepared using an ex situ CIS NP electrophoresis applied to a solution processed oxide nanostructure.[24] However, the conversion efficiency of those structures was quite low due to the imperfection of CIS penetration into the bottom of ZnO nanorods and the effect of interfacial structure was rarely discussed.

Herein, we describe a synthetic route to a $CuInS_2$/CdS/ZnO NR superstrate structure for use in a thin film solar cell. The device configuration is illustrated in Scheme 1. The densely

Scheme 1. Schematic Diagram of a Superstrate NR Solar Cell (ITO/ZnO seed/ZnO NRs array/CdS/$CuInS_2$ film/Au)

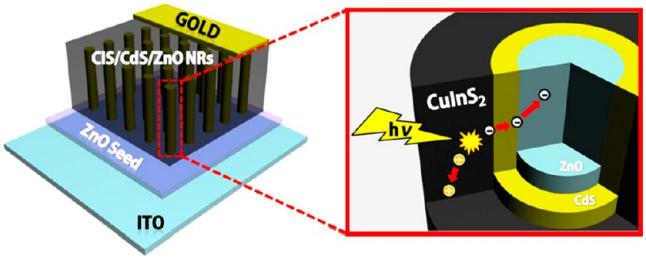

packed CdS/ZnO NRs with CIS were fabricated for the efficient separation and transport of photogenerated electrons and holes. All synthetic methods proceeded through non-vacuum routes. $CuInS_2$ provides a promising candidate with a direct band gap of 1.50 eV, which closely matches the best band gap yet achieved among solar cell materials (1.45 eV).[25] A ZnO template was prepared by fabricating hydrothermally grown transparent vertically aligned ZnO NR arrays. A CdS buffer layer was deposited using successive ion layer adsorption and reaction (SILAR) or nanocrystal layer deposition (NCLD) methods. After modifying the ZnO NR surfaces with CdS, solution-processed CIS was applied to CdS/ZnO NR arrays using a nontoxic molecular precursor solution to form p−n bulk heterojunctions.[26] The morphologies and crystal phases of the nanostructures and the complete solar cell structures were studied by scanning electron microscopy (SEM), X-ray diffraction (XRD), and energy-dispersive X-ray spectroscopy (EDX) analysis. The optoelectronic properties were collected using UV−vis spectroscopy, and the planar cell and NR cell were submitted to performance comparison studies. Also, to optimize the photovoltaic performances, the effects of CdS deposition process were studied. The method described here relies on low-temperature solution methods. This approach opens a variety of possibilities for the development of low-cost flexible thin film solar cells.

2. EXPERIMENTAL SECTION

Materials. All chemicals were purchased from Sigma-Aldrich and were used as received. Zinc nitrate hexahydrate ($Zn(NO_3)_2{\cdot}6H_2O$, 98%), ammonium hydroxide (28 wt % NH_3 in water, 99.99%), cadmium sulfate ($CdSO_4$, 99%), sodium sulfide (Na_2S, 98%), cadmium chloride ($CdCl_2$, technical grade), thioacetamide (C_2H_5NS, 99%), copper iodide (CuI, 99.999%), indium acetate ($In(OAc)_3$, 99.99%), thiourea (CH_4N_2S, 99%), 1-butylamine ($C_4H_9NH_2$, 99.5%), and 1-propionic acid (C_2H_5COOH, 99.5%) were used. Prior to material deposition, soda lime glass (SLG) substrates were ultrasonically cleaned for 10 min with detergent, acetone, and ethanol, respectively.

Preparation of the ZnO Nanorod Arrays. Prior to the growth of the ZnO nanorods (NRs), an ITO film was deposited onto the ultrasonically cleaned SLG at room temperature by RF-magnetron sputtering under a working pressure of 7 mTorr and an RF power of 100 W. The deposition time was 35 min. The sheet resistance of the sputtered ITO film was measured and found to be 8.6 Ω/□. Vertically aligned ZnO NRs were grown hydrothermally on the ZnO seed/ITO/SLG substrate.[27] The ZnO (∼50 nm) sputtered substrate was immersed in a beaker containing 10 mM $Zn(NO_3)_2{\cdot}6H_2O$ in water and 2 mL of ammonium hydroxide (28−30 wt %) and kept in an oven at 95 °C for 1 h. After the ZnO NW growth, the sample was cleaned several times with deionized water to remove any precipitates, followed by drying in air.

Deposition of the CdS Buffer Layer. A CdS buffer layer was coated onto the surface of the ZnO NR arrays using the SILAR method.[21] For the SILAR process, a 200 mM aqueous $CdSO_4$ and Na_2S solution was prepared. The substrate was successively immersed in $CdSO_4$ and Na_2S solutions for 30 s. Between each immersion, the substrate was rinsed with deionized water for 30 s to remove weakly bonded ions from the NR surfaces. This immersion−rinsing−immersion−rinsing cycle was repeated for 40 cycles. As the deposition cycle was repeated, the transparent sample gradually became yellow. After the SILAR deposition process, the substrate was dried in air.

The NCLD method was applied as reported previously to coat the ZnO surfaces with a CdS buffer layer.[28] Equal amounts of an aqueous precursor solution containing 20 mM $CdCl_2$ and 20 mM thioacetamide were mixed, and the samples were placed in a precursor solution for 25 min at room temperature. After the reaction, the samples were cleaned several times with water and dried in air.

Fabrication of the Photovoltaic Devices. A molecular precursor solution involving less toxic solvents was used to deposit a CIS film onto the CdS-coated ZnO NR arrays.[26] CuI (0.5715 g), $In(OAc)_3$ (0.971 g), thiourea (0.628 g), 1-butylamine (20 mL), and 1-propionic acid (1.3 mL) were mixed together and stirred for 10 min. The Cu:In:S ratio was adjusted to 0.9:1:2.5 to obtain the appropriate In and S-rich stoichiometry. The transparent sky-blue precursor solution was spin-coated onto the CdS/ZnO NR array samples at 1300 rpm for 30 s. The samples were then placed on a preheated 150 °C hot plate for 10 min. Without cooling, the heated sample was immediately moved to a preheated 250 °C hot plate and maintained at this temperature for 10 min. After heat treatment, the samples were allowed to cool to room temperature in an air environment. To complete the solar cell devices, we deposited a 100 nm thick patterned Au film by RF-magnetron sputtering. Finally, silver paste was squeezed onto Au and ITO electrodes and dried in air. The total active area was 0.20 cm^2.

Characterization. The morphologies of the nanostructures and films were investigated using field emission scanning electron microscopy (FE-SEM, XL30S, Philips). The crystal structural properties were analyzed by X-ray diffraction studies (XRD, Max-2500 V, RIGAKU). The optical properties of the nanostructures were evaluated by measuring the transmittance and absorbance spectra by UV−visible spectroscopy (JASCO, V-530). The performances of the solar cells were measured using a solar simulator equipped with a 300 W xenon lamp (Newport, USA) and a source meter (Keithley 2400). The power of the simulated light was calibrated to AM 1.5 (100 mW/cm^2) using a standard silicon solar cell (PV Measurement Inc.)

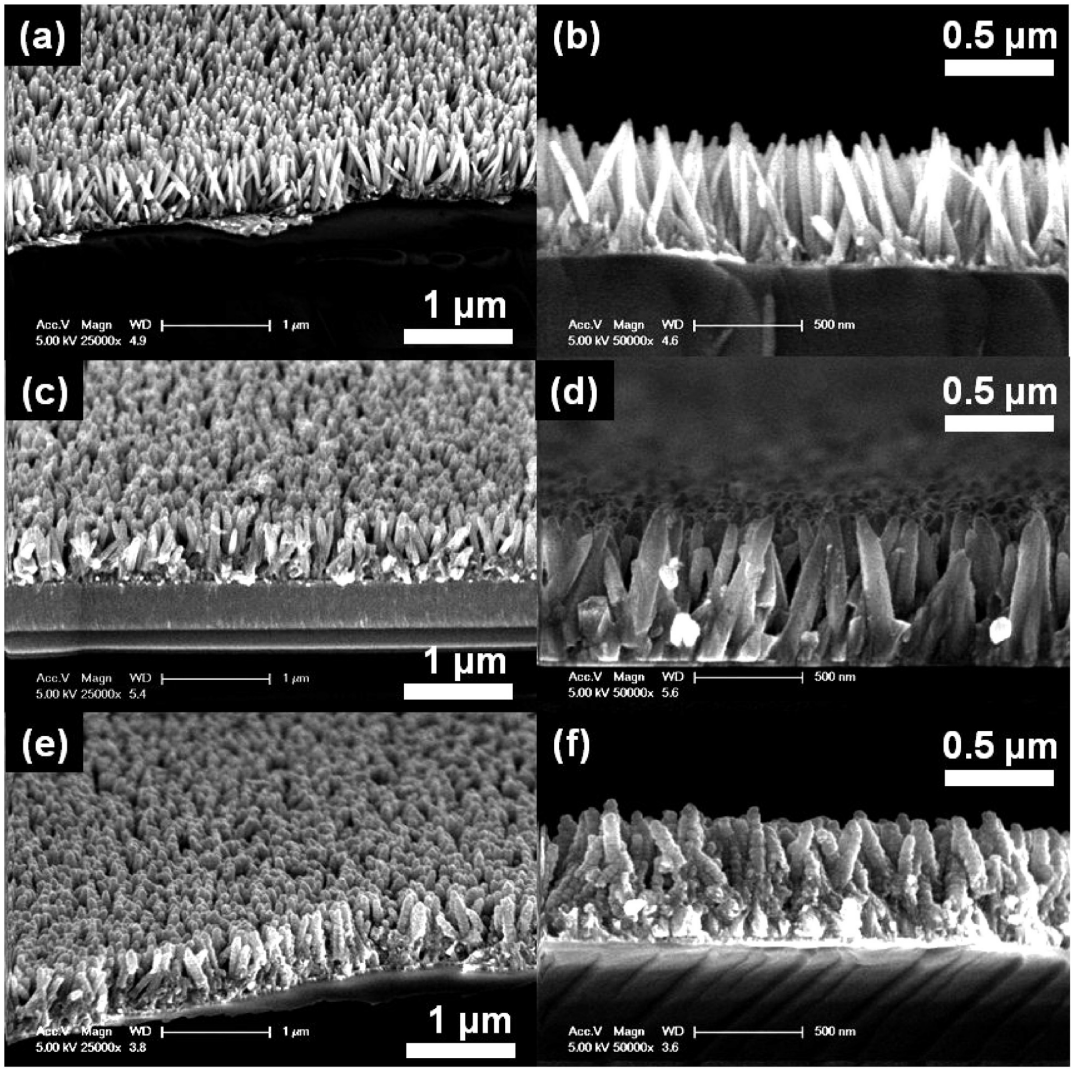

Figure 1. (a, c, e) Tilted and (b, d, f) cross-sectional SEM images of (a, b) as-grown ZnO NRs, (c, d) CdS-coated ZnO NRs prepared via 40 cycles of SILAR deposition, and (e, f) CdS-coated ZnO NRs prepared via NCLD.

3. RESULTS AND DISCUSSION

Figure 1 shows SEM images displaying the morphological changes in the ZnO NRs before and after CdS deposition. SILAR and NCLD processes were used for CdS deposition onto the ZnO NR arrays. Prior to the growth of ZnO NRs, the ITO back contact and ZnO seed films were sputtered onto the ultrasonically cleaned SLG substrate. Uniform ZnO NR arrays were synthesized at 95 °C within a short reaction time (1 h), as shown in Figure 1a. Control over the dimensions (e.g., length, diameter, degree of alignment) of the NRs was achieved by optimizing the precursor concentration, dipping time, and reaction temperature. It is related to the stabilization of the Zn ions in the precursor solution.[29,30] In this study, we added 2 mL of an ammonium hydroxide solution to the Zn precursor solution (pH ∼ 10.5), and a 1 h reaction time was used to obtain short-length NR arrays. As a result, an array of pristine ZnO NRs 500−600 nm in length and 40−50 nm in diameter was produced. Under low concentrated ammonium hydroxide (NH_4OH) conditions, homogeneous nucleation in bulk phase solution rapidly consume the Zn-amine complexes ($Zn(NH_3)_4^{2+}$) and inhibit the axial growth of the ZnO NRs because the amounts of $Zn(NH_3)_4^{2+}$ are deficient to induce heterogeneous nucleation on ZnO seed layer. On the contrary, in high concentrated NH_4OH solution, large amounts of $Zn(NH_3)_4^{2+}$ complexes react with hydroxyl anion (OH^-) in aqueous solution and produce ZnO crystals at elevated temperature. Thus, the growth rate of the ZnO NRs can be controlled by adjusting the amount of added ammonium hydroxide in solution.

In a CIGS solar cell, the introduction of a buffer layer improves the junction properties between an absorber and a window layer.[31,32] Buffering techniques are often used to inhibit the formation of interface traps and defect states that act as recombination centers in solution-grown junctions and decrease V_{oc}.[33] Generally, in a CIGS solar cell, the n-type CdS is extensively employed as a buffer layer to provide electrical advantages. CdS buffer layers can be helpful to enhance the device performances by avoiding undesirable shunt path and widening the depletion width that extend electric field in absorber layer and minimize the collection loss by tunneling and recombination.[34,35] In this study, the SILAR and NCLD methods were used to prepare a CdS/ZnO coaxial nanostructure. The SILAR technique is based on the ion-by-ion growth of sequentially adsorbed cations and anions at low temperatures; therefore, the film thickness can be controlled and a

conformal coating can be achieved. As shown in Figure 1b, up to 40 SILAR cycles yielded a 20 nm CdS shell layer deposited onto the ZnO NRs without significant longitudinal growth. A more detailed description of the CdS SILAR technique is discussed in our previous report.[22]

As shown in Figure 1c, in addition to SILAR, NCLD was used to deposit a CdS buffer layer. The NCLD technique, developed by Spoerke et al., is a modified chemical bath deposition (CBD) approach that enables the selective deposition onto ZnO surfaces at room temperature.[28] The conventional synthetic routes to CdS deposition in CIGS thin film solar cells generally have been based on CBD using an ammonia or NaOH-contained aqueous precursor solution to stabilize the Cd ions in the basic solution.[35] ZnO nanostructures can suffer from leaching problems under both low and high pH conditions because ZnO is an amphoteric compound and easily suffers from etching at the (0002) facet, which has a low surface energy.[36,37] Additionally, isolated CdS particle growth was generally observed, rather than ZnO-CdS core–shell coaxial structures. These surfaces were thought to form via a cluster–cluster mechanism by those CBD precursor combinations.[37,38]

The pH of the NCLD precursor solution containing $CdCl_2$ and thioacetamide was 5.5–6, thereby minimizing the deterioration of the ZnO surface. We observed the selective conformal growth of CdS only at the ZnO NRs, and no deposition was observed on the ITO or beaker surfaces. Spoerke et al. deposited that the ZnO surface, heavily decorated with surface-bound cadmium hydroxide complexes, was capable of reacting with thioacetamide to form a CdS layer, which nucleated directly on the ZnO.[28] After 25 min, the NCLD process yielded a 20–25 nm CdS shell layer on the surface of the ZnO NRs, with preservation of the ZnO core, as shown in Figure 1c.

XRD measurements were used to investigate the crystal structures of the bare ZnO NRs and the CdS-deposited ZnO NRs. Prior to CdS deposition, two main peaks corresponding to ZnO (002) and ZnO (103) were confirmed at 34.4 and 62.9° (JCPDS-792205), as shown in Figure 2a. CdS deposition via SILAR or NCLD produced different crystal phases in the deposited CdS. The CdS layer deposited by SILAR shows a broad peak at 26.5°, corresponding to cubic CdS (111) (JCPDS-800019) (Figure 2b). On the other hand, CdS layer grown via the NCLD method produced a polycrystalline hexagonal CdS phase with peaks corresponding to (100), (002), and (101) at 25.0, 26.6, and 28.3°, respectively (JCPDS-411049) (Figure 2c). The hexagonal CdS peaks were narrower compared to those of the SILAR-processed CdS peaks.

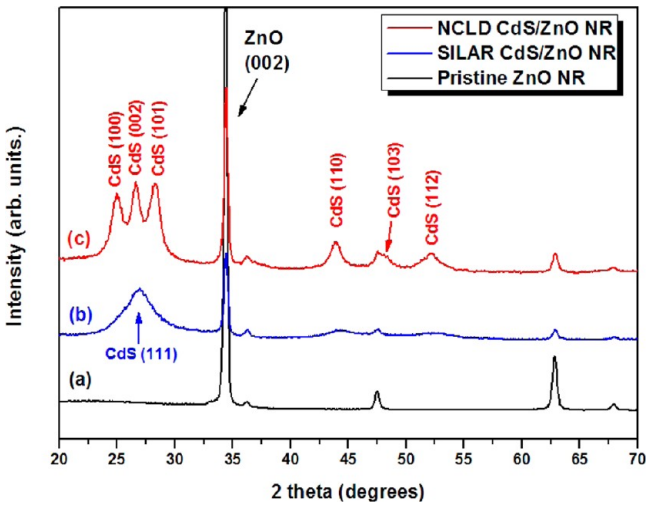

Figure 2. XRD patterns of nanostructures obtained through various deposition routes. (a) Pristine ZnO NRs, (b) SILAR 40 cycle CdS/ZnO NRs, and (c) NCLD CdS/ZnO NRs.

CuI, $In(OAc)_3$, and thiourea were used here as the Cu, In, and S sources, respectively, for the deposition of the CIS absorber layer onto the CdS/ZnO NRs. As solvents, 1-butylamine and 1-propionic acid were used to dissolve the metal precursors and form homogeneous transparent solutions. In the absence of 1-propionic acid, the metal precursors rapidly reacted with one another to form a brown precipitate upon injection into the amine solvent. The precursor solution was spin-coated onto the CdS-coated ZnO NR arrays in air at room temperature. The yellow colored substrate transformed into a semitransparent dark-brown film as the heat treatment progressed. As shown in Figure 3a, the as-spin-coated film showed a cubic $In(OH)_3$ XRD peak at 22.2° in addition to the

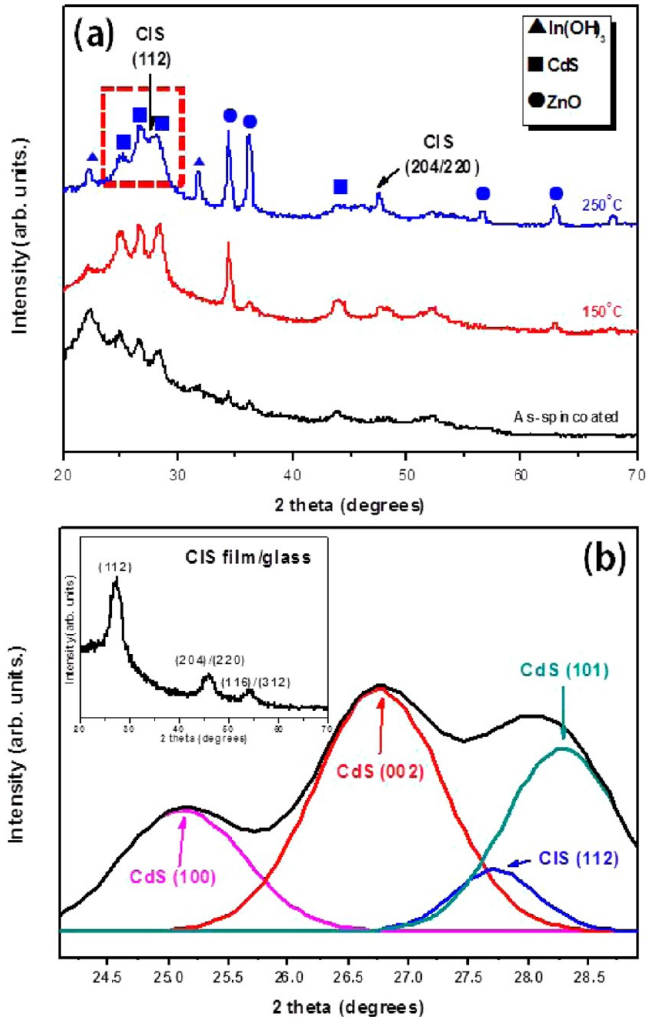

Figure 3. XRD patterns of the (a) ZnO NRs/NCLD CdS/CIS structure: as-spin-coated, annealed at 150 °C, and annealed at 250 °C in air. (b) Deconvolution results of a magnified XRD peak, assuming four Gaussian functions, revealing the presence of a CIS (112) peak among hexagonal CdS peaks. Inset shows the formation of chalcopyrite CIS phase on a glass substrate.

dx.doi.org/10.1021/am301957d | ACS Appl. Mater. Interfaces 2012, 4, 6758–6765

CdS and ZnO peaks (JPCDS-761464). Even after drying at 150 °C, the XRD pattern remained indistinguishable from that of the as-spin-coated film. These results indicated that the Cu, In, and S precursors did not react at temperatures up to 150 °C. The peak intensities of the CdS and ZnO increased slightly due to evaporation of the solvent and stabilizer, which has boiling points of 78 and 141 °C, respectively. Annealing in air at 250 °C, the temperature at which pure thiourea or metal−thiourea complexes begin to decompose, resulted in the formation of a CIS with preservation of the CdS and ZnO template (JCPDS-750106).[39]

A deconvolution method, assuming Gaussian functions, was used to fit the raw XRD profile (Figure 3b). The best fitting results were obtained for the four peaks corresponding to CdS (100), (002), (101), and for the CIS (112) peak appearing at 27.9°. The broad CIS (112) peak with a low intensity indicated small CIS crystal grain sizes due to the lack of a thermodynamic driving force for the sintering of adjacent crystallites at relatively low process temperatures. To provide the convincing proof of the formation of CIS chalcopyrite phase by our precursor solution method, we additionally confirmed the XRD pattern of CIS/glass sample. Inset of Figure 3b shows well-matched XRD pattern with reference CIS phase (JCPDS-750106).

The presence of residual $In(OH)_3$ from the In-rich precursor solution was also observed in the XRD pattern. If the residual byproducts were present in the absorber film, these byproducts could degrade the solar cell performance; therefore, further efforts were required to remove any undesired residual compounds. The selenization of sulfide crystals, which induces lattice volume expansion by substituting selenium for the small sulfur atoms, has been developed to produce dense absorber films and eliminate void space.[9,20] At this stage of development, further improvements in the crystal growth are required, and such improvements are currently under investigation.

Although the CIS (112) peak was concealed by relatively strong CdS peaks, the calculated average grain size of the CIS absorber film was estimated to be 8.5 nm using the Scherrer equation

$$D = 0.94\lambda/\beta\cos\theta$$

where D is the average crystallite size of the film, λ is the wavelength of incident X-rays (0.154 nm), β is the width of the peak at half-maximum intensity for a specific phase in radians (fwhm), and θ is the center angle of the peak.

As shown in Figure 4a, an interpenetrating network was obtained after CIS deposition onto the CdS/ZnO NRs array. To complete the device structure, a 100 nm thick Au top contact layer was sputtered on top of the CIS layer. CIS thin films deposited from a sulfur-rich solution tend to be single-phase with a preferred (112) growth direction and good stoichiometry. The atomic concentrations of Cu, In, and S were measured using EDX. EDX spectra revealed that the ratio of Cu:In:S was 0.9:1:2.1, corresponding to a slightly Cu-deficient $CuInS_2$. Considering that the Cu:In:S precursor ratio was 0.9:1:2.5, an excess of In and S in the precursor solution may have been lost during the sintering process in the air environment.

The optical properties of our samples were evaluated based on the UV−visible spectroscopic analysis. The optical transmittance spectra were gathered over the range 300−1100 nm. The spectra shown in Figure 5a indicated that the as-grown transparent ZnO NR arrays showed a strong band-edge absorption at 370 nm and enhanced visible light transparency

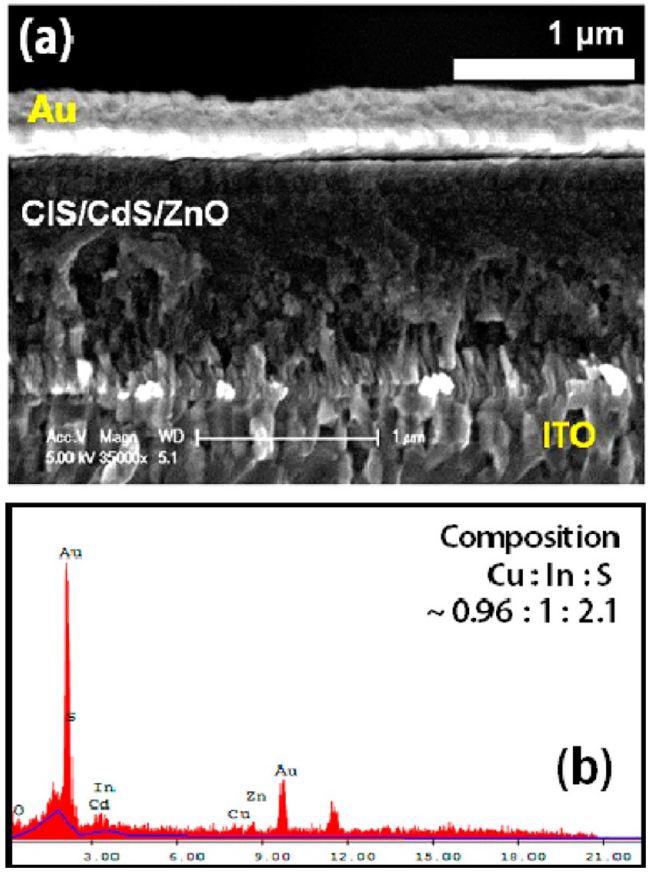

Figure 4. (a) SEM image of a complete superstrate solar cell device. A 100 nm thick gold film was deposited onto the completely infiltrated CIS/CdS/ZnO NRs. (b) EDX elemental analysis indicating a slightly Cu-poor stoichiometry in the CIS film.

compared to the flat 50 nm ZnO film. The color of the CdS-coated ZnO sample was yellow, and its absorption edge was observed at 500 nm, corresponding to the band gap energy of bulk CdS (2.4 eV).[40] Even after deposition of the CIS absorber, the sample appeared to be semitransparent, and the transmittance was reduced due to the absorption of photons with wavelengths greater than 850 nm. Figure 5b presents photographs of various samples.

Figure 6a shows the current density versus voltage curves under light illumination for the planar and nanostructured heterojunctions. The curves reveal the effects of the device structure and the quality of the buffer layer. The active area of the solar cells was 0.20 cm^2, and a 300 W Xe lamp was used as a light source. The best cell efficiency achieved here, using a cell with the SLG/ITO/ZnO seed/ZnO NRs/NCLD CdS/CIS/Au structure, yielded a power conversion efficiency of 3.30% with a short-circuit current density (J_{sc}), open-circuit voltage (V_{oc}), and fill factor (FF) of 10.1 mA/cm^2, 669.2 mV, and 49.4%, respectively.

Table 1 summarizes the photovoltaic performances of the CIS cells shown in Figure. 6(a). The NRs superstrate cells displayed a much higher solar energy conversion efficiency than was achieved in the flat heterojunction device. Compared to the planar device, NRs cell showed a remarkably enhanced J_{sc}. We attribute the enhanced J_{sc} to the reduced migration distance through NRs structure, giving rise to a rapid collection of minority carriers over the entire NRs.[41] In addition, improved light transmittance due to reduced reflective losses in the visible

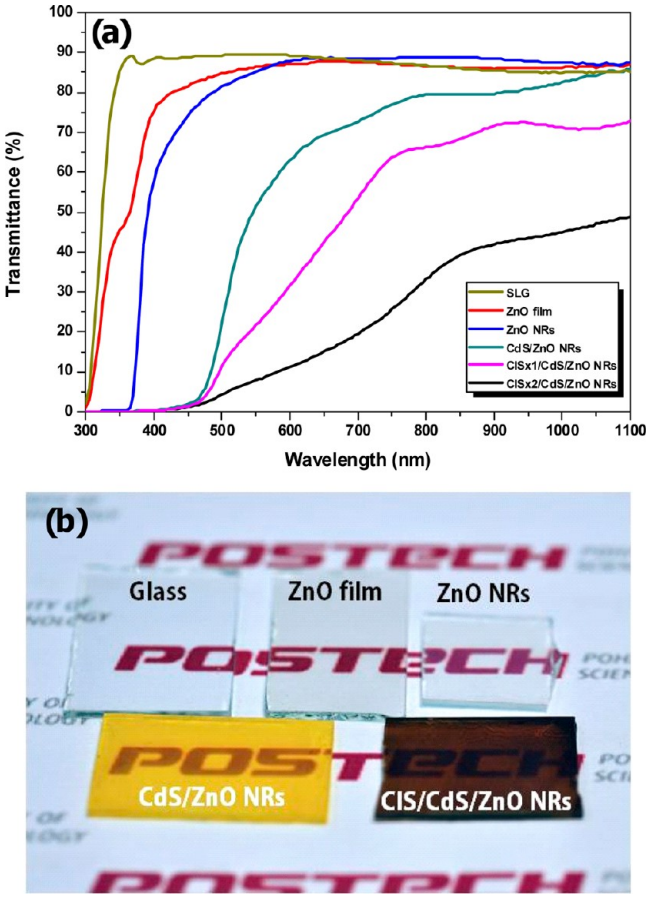

Figure 5. (a) UV−visible light transmittance spectra of samples of SLG, ZnO film, ZnO NRs, CdS-coated ZnO NRs, and CIS/CdS/ZnO NRs. CdS was deposited using the NCLD technique. (b) Photograph of each sample.

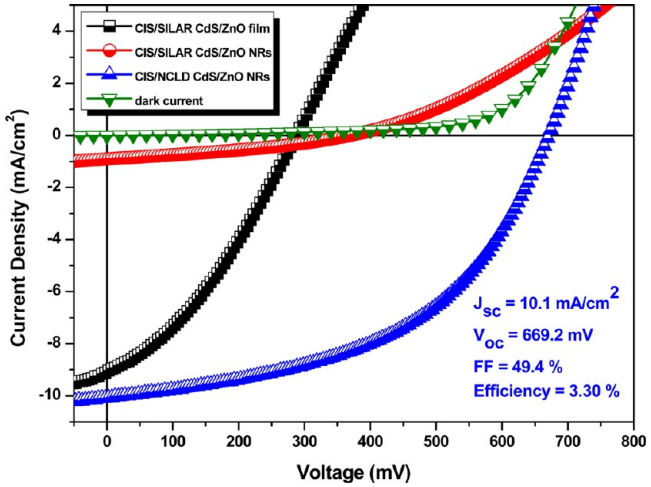

Figure 6. Dark and illuminated $J-V$ curves of the various structured heterojunctions. The performances of solar cells fabricated using a planar ZnO film or ZnO NRs were measured under AM 1.5 (100 mW/cm^2) conditions. Green triangle curve shows $J-V$ of CIS/NCLD CdS/ZnO NRs sample in dark condition.

region may further enhance the photoinduced current. However, a comparison of CdS SILAR-processed planar and nanostructured cells (cell 1 versus cell 2) reveals that the V_{oc} value for the SILAR CdS-coated NR cell was lower than that of

Table 1. Measured Values of J_{sc}, V_{oc}, FF, and the conversion efficiency for various device structures, obtained from the $J-V$ curve results

cell	cell structure	J_{sc} (mA/cm^2)	V_{oc} (mV)	FF (%)	active area (cm^2)	efficiency (%)
1	ZnO film/ SILAR 40c CdS/CIS	0.91	368.4	33.8	0.20	0.11
2	ZnO NR/ SILAR 40c CdS/CIS	9.1	288.2	33.9	0.20	0.89
3	ZnO NR/ NCLD CdS/ CIS	10.1	669.2	49.4	0.20	3.30

the planar cell. The nanostructured array generally yielded smaller V_{oc} values than the flat device. This was related to the distribution of the photoexcited minority carrier flux over the large junction area, rather than to the planar geometry.[42,43]

Theoretically, a small V_{oc} in a bulk heterojunction cell implies a reduced minority carrier flux across the junction boundary between the buffer/window layer and the absorber, if the rate of charge production is the same as that in a planar device. One difference in the V_{oc} values of nanostructured layers and planar layers results from the photocurrent density across the junction area. The V_{oc} of a nanostructured solar cell can be corrected by geometric factors related to its projected area according to the relationship

$$V_{oc} = (kT/q)[\ln(J_{sc}/J_0) - \ln \gamma]$$

where k is Boltzmann's constant, T is the temperature, q is the charge of electron, J_0 is the reverse saturation current density, and γ is the ratio between the junction area for a NR array and that of a flat film. γ may be expressed as

$$\gamma = \text{Area}_{NR}/\text{Area}_P$$
$$= (2\pi rh\rho_{NR} \times \text{Area}_P)/\text{Area}_P$$
$$= 2\pi rh\rho_{NR}$$

where Area_{NR} is the junction area of the NR array, Area_P is the area of the planar interface, r is the radius of a single NR, h is the height of a NR, and ρ_{NR} is the density of NRs. We estimated the extent of V_{oc} loss in a NR device, as compared to a planar device, using the values: r = 45−50 nm, h = 500−600 nm, and $\rho_{NR} \approx 10^{10}$ /cm^2. These parameters yield a γ value of 11−18, which will produce a V_{oc} loss of 60−75 mV. This value is on the order of the loss determined experimentally, as shown in Table 1.

We also conducted a dark current measurement to investigate recombination behavior of various device structures. Figure 7 shows plots of the logarithmic absolute dark current versus the applied voltage for the various device structures. The dark current measurements showed that the forward recombination current and reverse leakage current in a p−n junction diode could be qualitatively compared. Generally, a V_{oc} reduction in a thin film solar cell is attributed to leakage current and interfacial recombination.[44,45] In an NR device, the reverse and forward dark currents are higher than those in a flat device, suggesting several possible factors that contribute to V_{oc} loss. Because the leakage conduction of a thin film polycrystalline solar cell is generally not sufficient to affect the cell efficiency, the V_{oc} loss observed in our NR cell relative to the

dx.doi.org/10.1021/am301957d | ACS Appl. Mater. Interfaces 2012, 4, 6758−6765

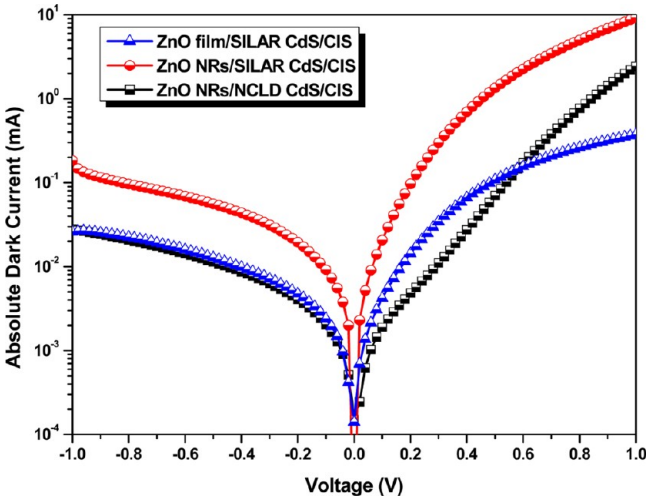

Figure 7. Absolute dark current versus applied voltage plot for the planar and nanostructured devices.

planar cell was thought to originate from the larger forward current under dark conditions. This suggests that recombination loss occurred frequently at the interfaces of the NR cells.[45]

According to Table 1, the quality of the CdS buffer layer significantly influenced the cell performance. The thickness of the NCLD CdS layer was comparable to that obtained through the 40 cycle SILAR process; however, the ZnO/NCLD CdS/CIS sample showed much higher values of J_{sc}, V_{oc}, FF, and power conversion efficiency. The improved V_{oc} photovoltaic response was attributed to the high quality of the CdS buffer layer fabricated via NCLD. This layer provided a much lower recombination probability during the efficient transfer of the generated charge carriers from the CIS to the CdS/ZnO. Depending on the synthetic route, CdS can have a metastable cubic phase or a highly stable hexagonal phase. Our results showed that the SILAR CdS assumed a cubic phase whereas NCLD produced hexagonal phase CdS. Hexagonal CdS films with columnar growth along the *c*-axis perpendicular to the substrate have been shown to have fewer grain boundaries parallel to the junction. Compared to the cubic phase CdS, hexagonal CdS displays better electrical conduction behavior, which can be understood by considering the larger crystallite size and reduced number of grain boundaries.[46] Although the CdS layer thickness in cells 2 and 3 were nearly identical, the dark current analysis shown in Figure 7 revealed that the recombination current in the NCLD CdS under a forward bias was much lower than that in a device containing SILAR-processed CdS/ZnO NRs. These results support our interpretation that a CdS buffer layer produced by NCLD is beneficial for cell performance. Hence, photogenerated charge carriers transfer efficiently through a hexagonal phase CdS buffer layer with reduced recombination. In the current study, cells 1 and 3 could not be directly compared because different CdS preparation methods were applied to different structured cells. A reasonable comparison may be made only among planar cells prepared with NCLD CdS; however, the conformal growth of CdS could not be achieved on the ZnO film using NCLD. The surface state or morphology of the ZnO film may affect the nucleation or growth of the CdS precipitate in the context of NCLD.

The cell performance of the SLG/ITO/ZnO seed/ZnO NRs/NCLD CdS/CIS/Au device can likely be further improved. The J_{sc} of our best cell was low, 10.1 mA/cm^2, because of the small grain size and the unnecessary CIS overlayer. A better photovoltaic performance may be achieved using film densification techniques, such as additional selenization or sintering at higher temperatures. These approaches will particularly improve J_{sc} and the FF. In addition, unnecessary overlayers, which typically increase the series resistance, should be minimized. A further study of the interfacial properties using Mott–Schottky analysis and/or impedance spectroscopy analysis can be used to characterize the electrical properties of the interfaces and composite structures.[33,47]

4. CONCLUSION

Low-temperature solution-based deposition routes for preparing ZnO NR arrays, a CdS buffer layer, and a CIS absorber layer, were combined to fabricate a superstrate CIS thin film solar cell. ZnO NRs were coated with a CdS buffer layer using either the SILAR or NCLD method. A precursor solution containing metal and sulfur precursors with a stabilizing agent was deposited onto the CdS-coated ZnO NR arrays, which were subsequently annealed in air to obtain a completely infiltrated CIS absorber layer in a CdS/ZnO NR array. The surface morphology and crystalline phase were analyzed at each synthesis step, and no noticeable interdiffusion of components was observed after thermal annealing at temperatures up to 250 °C. The advantages of the nanostructured devices over planar devices were demonstrated by comparing the optoelectronic properties and cell performances of planar and NR cells. The prepared ZnO NRs/NCLD CdS/CIS device exhibited the best efficiency of 3.30% because of the high material quality of the NCLD CdS and the efficient charge transfer through the large-area junction interface.

AUTHOR INFORMATION

Corresponding Author

*E-mail: kyong@postech.ac.kr.

Notes

The authors declare no competing financial interest.

ACKNOWLEDGMENTS

This research was supported by the Converging Research Center Program through the Ministry of Education, Science and Technology (2012K001273) and a grant from the National Research Foundation (NRF2010-0009545).

REFERENCES

(1) Aguilera, I.; Vidal, J.; Wahnón, P.; Reining, L.; Botti, S. *Phys. Rev. B* **2011**, *84*, 085145.
(2) Klenk, R.; Klaer, J.; Scheer, R.; Lux-Steiner, M. C.; Luck, I.; Meyer, N.; Rühle, U. *Thin Solid Films* **2005**, *480–481*, 509–514.
(3) Jackson, P.; Hariskos, D.; Lotter, E.; Paetel, S.; Wuerz, R.; Menner, R.; Wischmann, W.; Powalla, M. *Prog. Photovolt.* **2011**, *19*, 894–897.
(4) Lux-Steiner, M. C.; Ennaoui, A.; Fischer, C. H.; Jäger-Waldau, A.; Klaer, J.; Klenk, R.; Könenkamp, R.; Matthes, T.; Scheer, R.; Siebentritt, S.; Weidinger, A. *Thin Solid Films* **2000**, *361–362*, 533–539.
(5) Dhere, N. G. *Sol. Energy Mater. Sol. Cells* **2006**, *90*, 2181–2190.
(6) Hibberd, C. J.; Chassaing, E.; Liu, W.; Mitzi, D. B.; Lincot, D.; Tiwari, A. N. *Prog. Photovolt.* **2010**, *18*, 434–452.
(7) Todorov, T.; Mitzi, D. B. *Eur. J. Inorg. Chem.* **2010**, 17–28.
(8) Habas, S. E.; Platt, H. A. S.; van Hest, M. F. A. M.; Ginley, D. S. *Chem. Rev.* **2010**, *110*, 6571–6594.

(9) Lee, E.; Park, S. J.; Cho, J. W.; Gwak, J.; Oh, M. K.; Min, B. K. *Sol. Energy Mater. Sol. Cells* **2011**, *95*, 2928−2932.
(10) Wang, W.; Su, Y. W.; Chang, C. H. *Sol Energ Mat Sol C* **2011**, *95*, 2616−2620.
(11) Yuan, M.; Mitzi, D. B.; Gunawan, O.; Kellock, A. J.; Chey, S. J.; Deline, V. R. *Thin Solid Films* **2010**, *519*, 852−856.
(12) Ahn, S.; Kim, C.; Yun, J. H.; Gwak, J.; Jeong, S.; Ryu, B. H.; Yoon, K. *J. Phys. Chem. C* **2010**, *114*, 8108−8133.
(13) Lee, D.; Choi, Y.; Yong, K. *J. Cryst. Growth* **2010**, *312*, 3665−3669.
(14) Liu, W.; Mitzi, D. B.; Yuan, M.; Kellock, A. J.; Chey, S. J.; Gunawan, O. *Chem. Mater.* **2010**, *22*, 1010−1014.
(15) Chiang, M. Y.; Chang, S. H.; Chen, C. Y.; Yuan, F. W.; Tuan, H. Y. *J. Phys. Chem. C* **2011**, *115*, 1592−1599.
(16) Kind, C.; Feldmann, C.; Quintilla, A.; Ahlswede, E. *Chem. Mater.* **2011**, *23*, 5269−5274.
(17) Koo, B.; Patel, R. N.; Korgel, B. A. *J. Am. Chem. Soc.* **2009**, *131*, 3134−3135.
(18) Huang, W.-C.; Tseng, C.-H.; Chang, S.-H.; Tuan, H.-Y.; Chiang, C.-C.; Lyu, L.-M.; Huang, M. H. *Langmuir* **2012**, *28*, 8496−8501.
(19) Guo, Q.; Kim, S. J.; Kar, M.; Shafarman, W. N.; Birkmire, R. W.; Stach, E. A.; Agrawal, R.; Hillhouse, H. W. *Nano Lett.* **2008**, *8*, 2982−2987.
(20) Guo, Q.; Ford, G. M.; Hillhouse, H. W.; Agrawal, R. *Nano Lett.* **2009**, *9*, 3060−3065.
(21) Tak, Y.; Hong, S. J.; Lee, J. S.; Yong, K. *J. Mater. Chem.* **2009**, *19*, 5945−5951.
(22) Huang, Q.; Zhou, G.; Fang, L.; Hu, L.; Wang, Z.-S. *Energy Environ. Sci.* **2011**, *4*, 2145−2151.
(23) Cho, J. W.; Park, S. J.; Kim, J.; Kim, W.; Park, H. K.; Do, Y. R.; Min, B. K. *ACS Appl. Mater. Interface* **2012**, *4*, 849−853.
(24) Zhang, J.; Que, W. X.; Shen, F. Y.; Liao, L. *Sol. Energy Mater. Sol. Cells* **2012**, *103*, 30−34.
(25) Chen, G.; Wang, L.; Sheng, X.; Liu, H.; Pi, X.; Yang, D. *J. Alloys Compd.* **2010**, *507*, 317−321.
(26) Li, L.; Coates, N.; Moses, D. *J. Am. Chem. Soc.* **2010**, *132*, 22−23.
(27) Tak, Y.; Yong, K. J. *J. Phys. Chem. B* **2005**, *109*, 19263−19269.
(28) Spoerke, E. D.; Lloyd, M. T.; Lee, Y. J.; Lambert, T. N.; McKenzie, B. B.; Jiang, Y. B.; Olson, D. C.; Sounart, T. L.; Hsu, J. W. P.; Voigt, J. A. *J. Phys. Chem. C* **2009**, *113*, 16329−16336.
(29) Yamada, A.; Miyazaki, H.; Chiba, Y.; Konagai, M. *Thin Solid Films* **2005**, *480−481*, 503−508.
(30) Rodriguez-Torres, I.; Valentin, G.; Lapicque, F. *J. Appl. Electrochem.* **1999**, *29*, 1035−1044.
(31) Lenzmann, F.; Nanu, M.; Kijatkina, O.; Belaidi, A. *Thin Solid Films* **2004**, *451*, 639−643.
(32) Grasso, C.; Burgelman, M. *Thin Solid Films* **2004**, *451*, 156−159.
(33) Musselman, K. P.; Marin, A.; Wisnet, A.; Scheu, C.; MacManus-Driscoll, J. L.; Schmidt-Mende, L. *Adv. Funct. Mater.* **2011**, *21*, 573−582.
(34) Johnson, P. K.; Pudov, A. O.; Sites, J. R.; Ramanathan, K.; Hasoon, F. S.; Tarrant, D. E. In *Conference Record of the Twenty-Ninth IEEE Photovoltaic Specialists Conference*; IEEE: Piscataway, NJ, 2002; pp 764−767.
(35) Contreras, M. A.; Romero, M. J.; Hasoon, B. T. E.; Noufi, R.; Ward, S.; Ramanathan, K. *Thin Solid Films* **2002**, *403*, 204−211.
(36) Janotti, A.; Van de Walle, C. G. *Rep. Prog. Phys.* **2009**, *72*, 126501−126530.
(37) Tak, Y.; Hong, S. J.; Lee, J. S.; Yong, K. *Cryst. Growth Des.* **2009**, *9*, 2627−2632.
(38) Pawar, S. M.; Pawar, B. S.; Kim, J. H.; Joo, O. S.; Lokhande, C. D. *Curr. Appl. Phys.* **2011**, *11*, 117−161.
(39) Fischereder, A.; Rath, T.; Haas, W.; Amenitsch, H.; Schenk, D.; Zankel, A.; Saf, R.; Hofer, F.; Trimmel, G. *ACS Appl. Mater. Interfaces* **2012**, *4*, 382−390.
(40) Ramanathan, K.; Contreras, M. A.; Perkins, C. L.; Asher, S.; Hasoon, F. S.; Keane, J.; Young, D.; Romero, M.; Metzger, W.; Noufi, R.; Ward, J.; Duda, A. *Prog. Photovolt.* **2003**, *11*, 225−230.
(41) Nanu, M.; Schoonman, J.; Goossens, A. *Nano Lett.* **2005**, *5*, 1716−1719.
(42) Spurgeon, J. M.; Atwater, H. A.; Lewis, N. S. *J. Phys. Chem. C* **2008**, *112*, 6186−6193.
(43) Musselman, K. P.; Marin, A.; Schmidt-Mende, L.; MacManus-Driscoll, J. L. *Adv. Funct. Mater.* **2012**, *22*, 2202−2208.
(44) Bhattacharya, R. N.; Hiltner, J. F.; Batchelor, W.; Contreras, M. A.; Noufi, R. N.; Sites, J. R. *Thin Solid Films* **2000**, *361*, 396−399.
(45) Sites, J. R.; Granata, J. E.; Hiltner, J. F. *Sol. Energy Mater. Sol. Cells* **1998**, *55*, 43−50.
(46) Liu, F. Y.; Lai, Y. Q.; Liu, J.; Wang, B.; Kuang, S. S.; Zhang, Z. A.; Li, J.; Liu, Y. X. *J. Alloys Compd.* **2010**, *493*, 305−308.
(47) Akhavan, V. A.; Goodfellow, B. W.; Panthani, M. G.; Steinhagen, C.; Harvey, T. B.; Stolle, C. J.; Korgel, B. A. *J. Solid State Chem.* **2012**, *189*, 2−12.